

Article

Not peer-reviewed version

Design of a Flexure-based Flywheel for Storage of Angular Momentum and Kinetic Energy

Patrick Flückiger , [Florent Cosandier](#) , [Hubert Schneegans](#) ^{*} , [Simon Henein](#)

Posted Date: 15 February 2024

doi: 10.20944/preprints202402.0837.v1

Keywords: flexure mechanism; flywheel; energy storage; angular momentum



Preprints.org is a free multidiscipline platform providing preprint service that is dedicated to making early versions of research outputs permanently available and citable. Preprints posted at Preprints.org appear in Web of Science, Crossref, Google Scholar, Scilit, Europe PMC.

Copyright: This is an open access article distributed under the Creative Commons Attribution License which permits unrestricted use, distribution, and reproduction in any medium, provided the original work is properly cited.

Disclaimer/Publisher's Note: The statements, opinions, and data contained in all publications are solely those of the individual author(s) and contributor(s) and not of MDPI and/or the editor(s). MDPI and/or the editor(s) disclaim responsibility for any injury to people or property resulting from any ideas, methods, instructions, or products referred to in the content.

Article

Design of a Flexure-Based Flywheel for Storage of Angular Momentum and Kinetic Energy

Patrick Flückiger¹, Florent Cosandier², Hubert Schneegans^{3*} and Simon Henein⁴

¹ Instant-Lab, EPFL; patrick.fluckiger@epfl.ch

² Instant-Lab, EPFL; florent.cosandier@epfl.ch

³ Instant-Lab, EPFL; hubert.schneegans@epfl.ch

⁴ Instant-Lab, EPFL; simon.henein@epfl.ch

* Correspondence: hubert.schneegans@epfl.ch

Abstract: The flywheel is a widespread mechanical component used for the storage of kinetic energy and angular momentum. It typically consists of a cylindrical inertia rotating about its axis on rolling bearings, which involves undesired friction, lubrication, and wear. This paper presents an alternative mechanism that is functionally equivalent to a classical flywheel while relying exclusively on limited-stroke flexure-joints. This novel 1-degree-of-freedom zero-stiffness mechanism has no wear and requires no lubrication: it is thus compatible with extreme environments, such as vacuum, cryogenics, or ionizing radiation. The mechanism is composed of two coupled pivoting rigid bodies whose individual angular momenta vary during motion but whose sum is constant at all times when the pivoting rate is constant. The quantitative comparison of the flexure-based flywheel to classical ones based on a hollow cylinder as inertia shows that the former stores typically 6 times less angular momentum and kinetic energy for the same mass while occupying typically 10 times more volume. The freedom of design of the shape of the rigid bodies offers the possibility of modifying the ratio of the kinetic energy stored versus angular momentum, which is not possible with classical flywheels. For example, a flexure-based flywheel with rigid pivoting bodies in the shape of thin discs stores 100 times more kinetic energy than a classical flywheel with the same angular momentum. A proof-of-concept prototype was successfully built and characterized in terms of reaction moment generation, which validates the presented analytical model.

Keywords: flexure mechanism; flywheel; energy storage, angular momentum

1. Introduction

1.1. Flywheel State-of-the-Art and Article Contributions

Flywheels are well established mechanical components that are able to store kinetic energy (in the form of rotational energy) as well as angular momentum. We define a *standard flywheel* as a rigid body which rotates around an axis that coincides with its centre of mass (COM) and parallel to one of its principal axes of inertia. Flywheels have many applications, such as smoothing power output, serving as an additional source of energy and generating reaction torques. The smoothing of power output is commonly found in reciprocating engines. Flywheels may serve as an additional auxiliary power source in the form of intermittent pulses (for a forging hammer for example) or as a single impulse (for powering up a tokamak or aircraft catapult for example). The generation of reaction torques comes from the flywheel's ability to store angular momentum and finds its use in attitude control systems, such as the reaction wheels and control moment gyros of spacecrafts.

A standard flywheel is fixed to its base by means of a rotating bearing, such as ball bearings, gas bearings or magnetic bearings, which permits multiple complete revolutions. This last property is what prevents flexures from being used as the flywheel's bearing. Indeed, flexures work by using elastic deformation of flexible members in the mechanism. They also have a limited stroke and therefore cannot directly replace the flywheel bearing as the latter must be able to perform multiple complete

revolutions. The challenge in using flexures is designing a mechanism that can act like a rotating flywheel with limited stroke in each joint.

This article proposes an alternative design of a flywheel that is compatible with the use of flexures, in the sense that this mechanism stores kinetic energy and generates angular momentum. In addition, a comparative study of performances is drawn between a standard flywheel and the proposed flexure design.

1.2. Requirements for a Flexure-Based Flywheel Equivalent

To establish criteria for a flexure-based flywheel equivalent, the key properties of a standard flywheel need to be highlighted. First, the flywheel's centre of mass remains fixed during its motion and therefore does not export any forces during motion. This property is defined as being *force balanced* by Schneegans et al. [1]. The flywheel is also in equilibrium when at rest (i.e., is not subject to any forces), regardless of its orientation, and therefore has a constant potential energy, a property defined as *statically balanced* by [1]. During its motion, the flywheel generates angular momentum that is constant in amplitude and in direction. Last, if the standard flywheel has a cylindrical shape, as in most cases, the inertia tensor of the flywheel, as seen from its base, does not change. If this is not the case and if the flywheel's base is also rotating, the flywheel will export torque. This last property, defined as *inertial invariance* by [1], is however regarded as optional as its effect will only be apparent for a flywheel whose base is rotating.

To allow the selection of an appropriate design, the properties described above are now enumerated:

1. The centre of mass of the reaction mechanism must remain fixed throughout its motion.
2. The mechanism must be able to generate angular momentum that is constant in direction.
3. The mechanism must be able to generate angular momentum that is constant in amplitude.
4. The mechanism must be able to control the amplitude of its angular momentum in order to deliver a reaction torque
5. The inertia tensor of the flywheel, as seen from its base, must remain constant throughout the motion. (Optional)

1.3. Outline of Paper

Section 2.1 defines the inertial bodies considered in this paper along with the definition of CV-joints and their notational conventions. The flexure-based flywheel and its working principle will then be presented with ideal joints in section 2.2. Even though this flywheel uses ideal joints (and therefore not necessarily flexures), it will still be referred to as a flexure-based flywheel to avoid additional terminology. In section 2.3.2, the kinetic energy and angular momentum of this mechanism will be discussed, followed by the internal forces that transit through the joints (section 2.4). In section 3, the comparative study between a standard flywheel and the flexure-based design will then be shown and their performances in terms of kinetic energy, angular momentum and volume will be discussed. Section 4 shows the influence of the shape ratio of pivoting cylindrical rigid bodies on the generation of angular momentum and storage of kinetic energy. Thereafter, we highlight in section 5 the analogy between the proposed mechanism and a falling cat. Last, in section 6, an example of a flexure implementation along with the constructed proof-of-concept prototype and experimental measurements will be shown.

2. Flexure-Based Flywheel

2.1. Definition of Specific Inertial Bodies and CV-Joint Kinematics

Before presenting the mechanism and its working principle, the types of inertial bodies present in this paper are introduced, along with the notion of *constant velocity joints* (CV-joints) and notational conventions used to describe their kinematics.

We define a *spherical inertial body* as a rigid body in which all three moments of inertia around its principal axes of inertia are identical. Its inertia tensor J_{sph} , when evaluated in the frame of its principle axes of inertia, is given by:

$$J_{\text{sph}} = \begin{bmatrix} J_{\text{sph}} & 0 & 0 \\ 0 & J_{\text{sph}} & 0 \\ 0 & 0 & J_{\text{sph}} \end{bmatrix} \quad (1)$$

We define a *cylindrical inertial body* as a rigid body in which two moments of inertia around its principle axes of inertia are identical and it is assumed that these two principle axes coincide with the x - and y -axes. Its inertia tensor J_{cyl} , when evaluated in the frame of its principal axes of inertia, is given by (J_h and J_v have been chosen as the notation to designate the moments of inertia around the 'horizontal' axes x and y , and moment of inertia around the 'vertical' z -axis.):

$$J_{\text{cyl}} = \begin{bmatrix} J_h & 0 & 0 \\ 0 & J_h & 0 \\ 0 & 0 & J_v \end{bmatrix} \quad (2)$$

A cylindrical inertial body is not necessarily a cylinder, but can take other shapes. A *dumbbell* is another embodiment of a cylindrical inertial body as it results in the same inertia tensor, as shown in Figure 1 (right).

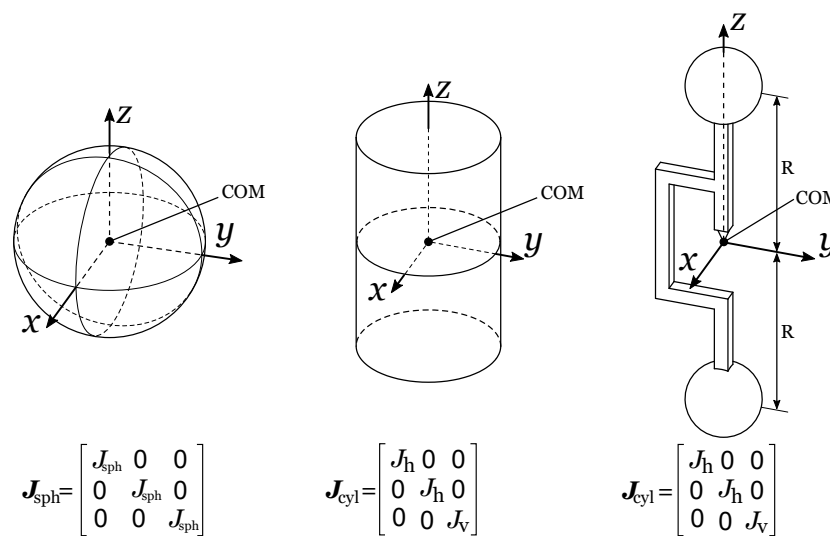


Figure 1. The inertial bodies considered in this paper: spherical inertial body (left), cylindrical inertial body (centre) and dumbbell (right). This dumbbell has its mass concentrated exclusively in the two sphere-shaped masses (the rigid arms linking them are neglected) and the dumbbell effectively acts as a cylindrical inertial body. The centre of mass (COM) of each body is highlighted and it is assumed that principal axes of inertia coincide respectively with the x -, y - and z -axes. It can be seen that the cylinder and dumbbell have the same inertia tensor.

The orientation of rigid bodies will be described using Euler angles. The convention for the three successive rotations is depicted in Figure 2 in which the body is first rotated around the z -axis by angle φ (azimuth), then rotated around n by angle θ (elevation), and finally around axis v by angle ψ (twist). Moreover, the notational convention we adopt for the rotation matrix describing a rotation α around an axis a is $R_a(\alpha)$. The rotation of a body is therefore given by the product $R_z(\varphi)R_y(\theta)R_z(\psi - \varphi)$. (Intuitively these rotations correspond to "apply twist and borrow azimuth for correct application of elevation", "apply elevation" and "apply azimuth". The notational convention

adopted in this paper differs from that of [2] in the sense that [2] regroups $\psi - \varphi$ into ψ . The authors prefer the adopted notation as it clearly identifies twist).

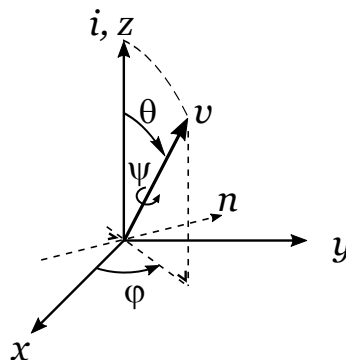


Figure 2. Sequential rotations with Euler angles φ , θ and ψ , designated respectively as azimuth, elevation and twist. The rotation sequence is first rotation φ around axis i , then rotation θ around n and finally rotation ψ around v

CV-joints are variants of the universal joint and are typically used for transmission of torque from one rotating shaft to another without any variation of speed. In this paper, these same CV-joints are in a different configuration, in which the input shaft is fixed and the output shaft has two rotational degrees of freedom. The kinematics of a CV-joint in terms of Euler angles have been described by Vardi et al. [2] who states that the joint has zero-torsion (i.e., $\psi = 0$). This means that the kinematics of a CV-joint are given by the product rotation matrix $\mathbf{R}_{CV}(\theta, \varphi)$:

$$\mathbf{R}_{CV}(\theta, \varphi) = \mathbf{R}_z(\varphi)\mathbf{R}_y(\theta)\mathbf{R}_z(-\varphi) \quad (3)$$

in which:

$$\mathbf{R}_z(-\varphi) = \begin{bmatrix} \cos \varphi & \sin \varphi & 0 \\ -\sin \varphi & \cos \varphi & 0 \\ 0 & 0 & 1 \end{bmatrix}; \mathbf{R}_y(\theta) = \begin{bmatrix} \cos \theta & 0 & \sin \theta \\ 0 & 1 & 0 \\ -\sin \theta & 0 & \cos \theta \end{bmatrix}; \mathbf{R}_z(\varphi) = \begin{bmatrix} \cos \varphi & -\sin \varphi & 0 \\ \sin \varphi & \cos \varphi & 0 \\ 0 & 0 & 1 \end{bmatrix} \quad (4)$$

2.2. Description of the Mechanism and Working Principle

As shown in Figure 3, the mechanism is composed of two identical cylindrical rigid bodies (1) and (2) which are each attached to a fixed base (3) via CV-joints (A), respectively (B) located at each body's centre of mass. The bodies (1) and (2) are connected with one-another via a ball joint (C) located at equidistance from (A) and (B) (i.e, the distances are such as $AC = BC$ and $AC + BC > AB$). This arrangement forces the centre of the ball joint (C) to remain at a constant distance from the AB line. As a result, when the mechanism moves, (C) follows a circular path, the elevation angles of the two CV-joints are equal and constant ($\theta_1 = \theta_2$) and the azimuth angles of the two CV-joints have a phase shift of π ($\varphi_1 = \varphi_2 + \pi$). This motion which keeps a fixed elevation and sweeps the azimuth shall be defined as the *pivoting motion*.

The working principle at play is that the angular momenta of each pivoting body are oblique. When the whole mechanism is considered, the x - and y -components of the angular momentum are cancelled out and only the constant z -component remains. This one degree-of-freedom mechanism is isostatic and when it moves, presents the following key properties:

1. 1 degree-of-freedom, i.e., the azimuth angle φ fully determines the position of both segments (1) and (2).

2. For a constant velocity: $\dot{\varphi} = \text{constant}$, the total angular momentum of the mechanism is constant.
3. The angular deflection of the two CV joints (A) and (B) in elevation remains constant at all times $\theta = \text{constant}$.
4. The angular deflection of the ball joint (C) in elevation ρ remains constant at all times and equal to $\rho = 2\theta = \text{constant}$.
5. If the joints (A), (B) and (C) have positive isotropic angular stiffnesses, then the elastic potential energy of the mechanism remains constant at all times and the mechanism is statically balanced (i.e., the mechanisms as a whole is zero-force).
6. If the rigid bodies (1) and (2) are in addition spherical rigid bodies, then the inertia tensor of the mechanism as whole remains constant at all time and condition 5 is fulfilled.

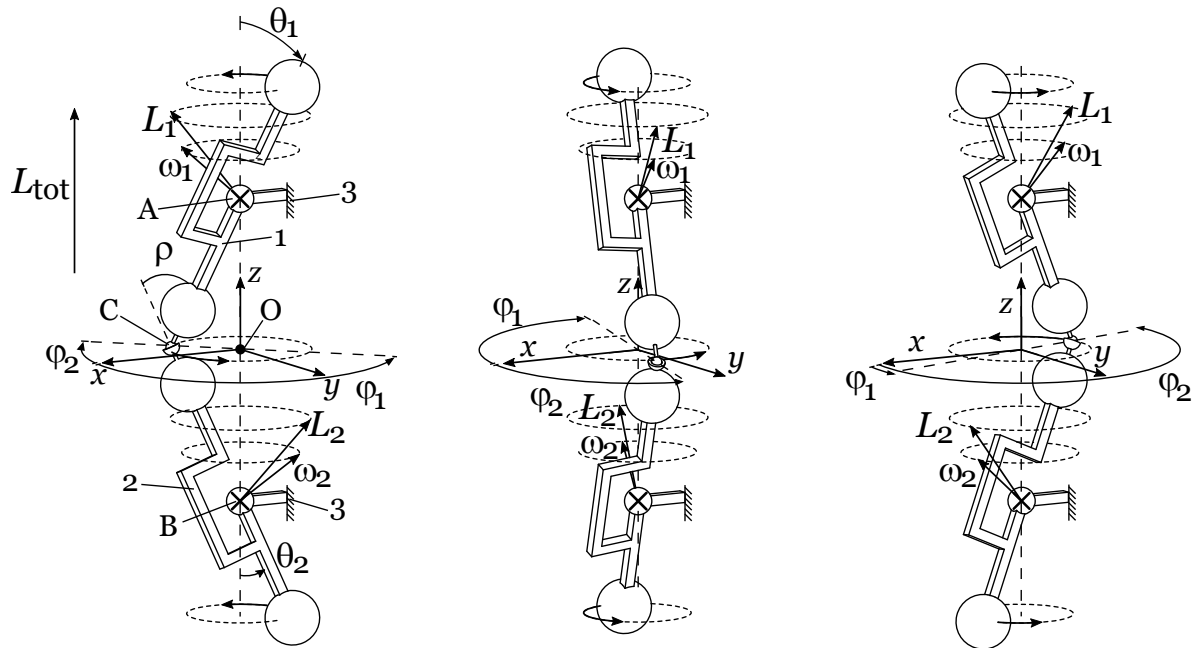


Figure 3. Sequence of the flywheel design. It can be seen that at each step the bodies' angular momenta L_1 and L_2 are oblique and result in a total angular momentum L_{tot} .

2.3. Kinematics

2.3.1. Kinematics of Rigid Body 1

Let \mathcal{R}_A be the inertial frame centered on (A) whose axes are parallel to the x -, y - and z -axes.

In rigid body 1's attached frame (coincident with its principal axes), rigid body 1's inertia tensor \mathbf{J}_{cyl} is given by Eq. (2). Following Eq. (3), the orientation of rigid body 1 is given by the rotation matrix $\mathbf{R}_{CV,1}$:

$$\mathbf{R}_{CV,1} = \mathbf{R}_{CV}(\theta, \varphi) \quad (5)$$

As seen in inertial frame \mathcal{R}_A , rigid body 1's inertia tensor $\mathbf{J}_{1,\mathcal{R}}$ is given by:

$$\mathbf{J}_{1,\mathcal{R}_A} = \mathbf{R}_{CV,1} \mathbf{J}_{cyl} \mathbf{R}_{CV,1}^T \quad (6)$$

Vardi [2] also provides a formula for the angular velocity of the pivoting rigid body 1, evaluated in \mathcal{R}_A . Vardi explains that when Euler angles are used, the angular velocity ω is given by

$$\omega = \dot{\varphi} \mathbf{i} + \dot{\theta} \mathbf{n} + \dot{\psi} \mathbf{v}, \quad (7)$$

which leads to:

$$\boldsymbol{\omega}_1 = \dot{\varphi} (\mathbf{i} - \mathbf{v}) = \dot{\varphi} \left(\begin{bmatrix} 0 \\ 0 \\ 1 \end{bmatrix} - \mathbf{R}_{CV,1} \begin{bmatrix} 0 \\ 0 \\ 1 \end{bmatrix} \right) = \dot{\varphi} \begin{bmatrix} -\cos \varphi \sin \theta \\ -\sin \varphi \sin \theta \\ (1 - \cos \theta) \end{bmatrix} \quad (8)$$

The angular momentum \mathbf{L}_1 of pivoting rigid body 1, evaluated in \mathcal{R}_A is then given by:

$$\mathbf{L}_1 = \mathbf{J}_{1,\mathcal{R}_A} \boldsymbol{\omega}_1 = \dot{\varphi} \begin{bmatrix} -\cos \varphi ((J_h - J_v) \cos \theta + J_v) \sin \theta \\ -\sin \varphi ((J_h - J_v) \cos \theta + J_v) \sin \theta \\ (1 - \cos \theta) ((J_h - J_v) \cos \theta + J_h) \end{bmatrix} \quad (9)$$

along with its kinetic energy K_1 :

$$K_1 = \frac{1}{2} \boldsymbol{\omega}_1^T \mathbf{J}_{1,\mathcal{R}_A} \boldsymbol{\omega}_1 = \frac{1}{2} \dot{\varphi}^2 (1 - \cos \theta) ((J_h - J_v) \cos \theta + J_v + J_h). \quad (10)$$

2.3.2. Kinematics of Rigid Body 2

Similarly as for rigid body 1, the rotation matrix $\mathbf{R}_{CV,2}$ for rigid body 2 is given by:

$$\mathbf{R}_{CV,2} = \mathbf{R}_{CV}(\theta, \varphi + \pi) \quad (11)$$

Let \mathcal{R}_B be the inertial frame centered on (B), whose axes are parallel to the x -, y - and z -axes. Rigid body 2's inertia tensor, as seen in inertial frame \mathcal{R}_B , is given by:

$$\mathbf{J}_{2,\mathcal{R}_B} = \mathbf{R}_{CV,2} \mathbf{J}_{\text{cyl}} \mathbf{R}_{CV,2}^T \quad (12)$$

The angular velocity of the pivoting inertial body 2, evaluated in \mathcal{R}_B is calculated in the same manner as inertial body 1:

$$\boldsymbol{\omega}_2 = \dot{\varphi} (\mathbf{i} - \mathbf{v}) = \dot{\varphi} \left(\begin{bmatrix} 0 \\ 0 \\ 1 \end{bmatrix} - \mathbf{R}_{CV,2} \begin{bmatrix} 0 \\ 0 \\ 1 \end{bmatrix} \right) = \dot{\varphi} \begin{bmatrix} \cos \varphi \sin \theta \\ \sin \varphi \sin \theta \\ (1 - \cos \theta) \end{bmatrix} \quad (13)$$

The angular momentum \mathbf{L}_2 of pivoting inertial body 2, evaluated in \mathcal{R}_B , is then given by:

$$\mathbf{L}_2 = \mathbf{J}_{2,\mathcal{R}_B} \boldsymbol{\omega}_2 = \dot{\varphi} \begin{bmatrix} \cos \varphi ((J_h - J_v) \cos \theta + J_v) \sin \theta \\ \sin \varphi ((J_h - J_v) \cos \theta + J_v) \sin \theta \\ (1 - \cos \theta) ((J_h - J_v) \cos \theta + J_h) \end{bmatrix}, \quad (14)$$

whose z component is similar as the one of \mathbf{L}_1 . Likewise, its kinetic energy K_2 is:

$$K_2 = \frac{1}{2} \boldsymbol{\omega}_2^T \mathbf{J}_{2,\mathcal{R}_B} \boldsymbol{\omega}_2 = \frac{1}{2} \dot{\varphi}^2 (1 - \cos \theta) ((J_h - J_v) \cos \theta + J_v + J_h), \quad (15)$$

which equals the kinetic energy K_1 of inertial body 1.

2.3.3. Angular Momentum and Kinetic Energy of the Complete Mechanism

As the centres of mass of rigid bodies 1 and 2 remain fixed during the pivoting motion, their angular momenta do not depend on which inertial frame is used. As for their kinetic energies, it is always independent of the considered inertial frame. For ease, we will evaluate the complete

mechanism in the inertial frame \mathcal{R}_0 centered on O and whose axes coincide with the x -, y - and z -axes. The complete mechanism's angular momentum \mathbf{L}_{tot} , evaluated in \mathcal{R}_0 , is then:

$$\mathbf{L}_{\text{tot}} = \mathbf{L}_1 + \mathbf{L}_2 = \dot{\varphi} \begin{bmatrix} 0 \\ 0 \\ 2(1 - \cos \theta) ((J_h - J_v) \cos \theta + J_h) \end{bmatrix} \quad (16)$$

It can be seen that in order to develop a maximum of angular momentum, it is advantageous to increase the elevation θ and to opt for long and slender cylindrical bodies (as this increases J_h and decreases J_v). From here, we can introduce $J_{\text{equ,L}}$: the *angular momentum equivalent moment of inertia*, defined as (The interest of $J_{\text{equ,L}}$ is to evaluate how much angular momentum is generated as a function of the pivoting rate $\dot{\varphi}$):

$$J_{\text{equ,L}} = \frac{\mathbf{L}_{\text{tot}} \cdot \mathbf{z}}{\dot{\varphi}} = 2(1 - \cos \theta) ((J_h - J_v) \cos \theta + J_h) \quad (17)$$

The kinetic energy K_{tot} of the complete mechanism is given by:

$$K_{\text{tot}} = K_1 + K_2 = \dot{\varphi}^2 (1 - \cos \theta) ((J_h - J_v) \cos \theta + J_v + J_h) \quad (18)$$

From this, we can introduce $J_{\text{equ,K}}$: the *kinetic energy equivalent moment of inertia*, defined as (The interest of $J_{\text{equ,K}}$ is to evaluate how much kinetic energy is generated as a function of the pivoting rate $\dot{\varphi}$):

$$J_{\text{equ,K}} = \frac{2K_{\text{tot}}}{\dot{\varphi}^2} = 2(1 - \cos \theta) ((J_h - J_v) \cos \theta + J_v + J_h) \quad (19)$$

2.4. Joint sollicitation through internal forces

This section evaluates the internal forces that transit through the CV-joints and ball-joint in the stationary case (i.e., $\dot{\varphi}$ is constant). The approach is to isolate one of the pivoting rigid bodies (rigid body 1 is chosen for this example) and to determine the net torque and force that are applied to it. The net torque applied to rigid body 1 is determined by calculating the time variation of its angular momentum $\dot{\mathbf{L}}_1$:

$$\dot{\mathbf{L}}_1 = \dot{\varphi}^2 \sin \theta ((J_h - J_v) \cos \theta + J_v) \begin{bmatrix} \sin \varphi \\ -\cos \varphi \\ 0 \end{bmatrix} \quad (20)$$

This vector lies within the xy -plane, has a constant amplitude and rotates at a fixed rate around the z -axis, as shown in Figure 4. Indeed, the net torque \mathbf{M}_1 applied to rigid body 1 equals $\dot{\mathbf{L}}_1$:

$$\mathbf{M}_1 = \dot{\mathbf{L}}_1 \quad (21)$$

Concerning the net force applied to rigid body 1, since its centre of mass remains fixed during motion, the applied net force is zero. Moreover, due to symmetry considerations, the internal force \mathbf{T} transiting through the ball joint, applied by rigid body 2 onto rigid body 1, is parallel to the z -axis. This means that the CV-joint applies a force $\mathbf{T}' = -\mathbf{T}$, also parallel to the z -axis, onto rigid body 1 and that \mathbf{T} and \mathbf{T}' form together a couple. As flexures are to be used in this flywheel, it can be assumed that the CV-joints and ball-joint have isotropic (isotropic in the sense that the stiffness does not vary with φ ,

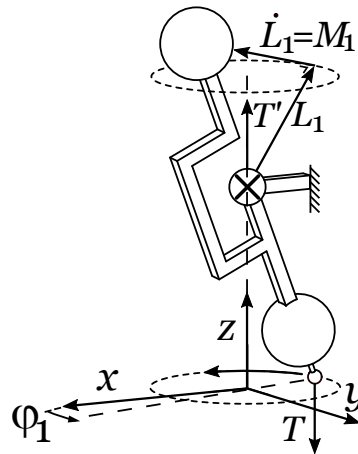


Figure 4. Rigid body 1 isolated from the rest of the mechanism. The internal forces \mathbf{T} and \mathbf{T}' are applied respectively to its ball-joint and CV-joint. The net torque \mathbf{M}_1 , equal to $\dot{\mathbf{L}}_1$, the time derivative of \mathbf{L}_1 , is also highlighted.

i.e., that the stiffness is the same for all tilting directions.) angular stiffnesses k_A and k_C respectively. The net torque \mathbf{M}_1 is given by:

$$\mathbf{M}_1 = (k_A\theta + k_C(2\theta)) \begin{bmatrix} \sin \varphi \\ -\cos \varphi \\ 0 \end{bmatrix} + \begin{bmatrix} -R \sin \theta \cos \varphi \\ -R \sin \theta \sin \varphi \\ -R \cos \theta \end{bmatrix} \times \mathbf{T} \quad (22)$$

$$= (TR \sin \theta + k_A\theta + k_C(2\theta)) \begin{bmatrix} \sin \varphi \\ -\cos \varphi \\ 0 \end{bmatrix}, \quad (23)$$

with T the amplitude of force $\mathbf{T} = [0, 0, -T]^T$. From Eqs. (20), (21) and (23), the amplitude T of force \mathbf{T} is given by:

$$T = \frac{\dot{\varphi}^2 \sin \theta ((J_h - J_v) \cos \theta + J_v) - k_A\theta - k_C(2\theta)}{R \sin \theta}. \quad (24)$$

An interesting property is that this force increases with $\dot{\varphi}^2$, which resemble the behaviour of a centripetal force. Another notable property of this formula is that the joints' stiffnesses, which can be viewed as a preload, reduce the effective joint sollicitation.

3. Comparison of a dumbbell flexure design to a standard flywheel

This section compares the angular momentum and kinetic energy of the flexure-based flywheel to those of a standard flywheel. The standard flywheel selected as a benchmark for this comparison is a hollow cylinder, whose thickness to radius ratio ζ is fixed to 0.1 (see Figure 5):

$$\zeta = \frac{2w}{D} = \frac{1}{10}. \quad (25)$$

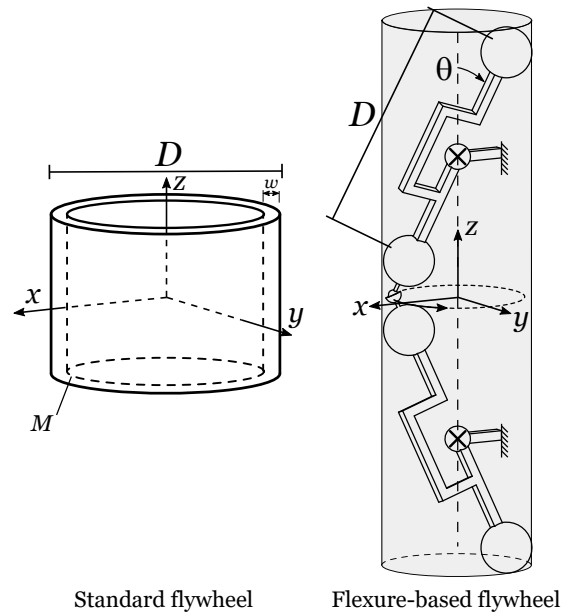


Figure 5. Standard flywheel and flexure-based flywheel used for the performance comparison. The standard flywheel's diameter D matches the dumbbell's length (i.e., the distance between the centres of the sphere-shaped masses). The cylindrical envelope of the flexure-based flywheel is also highlighted and encompasses the whole mechanism, including the dumbbells' spheres.

To allow a comparison to be drawn, both the flexure-based and standard designs have the same total mass M and the dumbbell's length $2R$ matches the flywheel's diameter D , as shown in Figure 5.

The moment of inertia of the standard flywheel is given by:

$$J_{\text{std}} = \frac{MD^2 (\xi^2 - 2\xi + 2)}{8}. \quad (26)$$

Moreover, in order to reach the correct mass M , this standard flywheel has a height H given by:

$$H = \frac{4M}{\rho\pi D^2 \xi (2 - \xi)}, \quad (27)$$

resulting in an envelope volume V_{std} given by:

$$V_{\text{std}} = \pi \left(\frac{D}{2}\right)^2 H = \frac{M}{\rho \xi (2 - \xi)}. \quad (28)$$

For the compared flexure design, the sphere-shaped masses m and their radii r are given by:

$$m = \frac{M}{4} \quad \text{and} \quad r = \left(\frac{3m}{4\pi\rho}\right)^{\frac{1}{3}}, \quad (29)$$

with ρ the material's density. This yields:

$$J_{\text{h}} = 2m \cdot \left(\frac{2}{5}r^2 + \left(\frac{D}{2}\right)^2\right) \quad \text{and} \quad J_{\text{v}} = \frac{4}{5}mr^2. \quad (30)$$

Moreover, the cylindrical envelope of this dumbbell design, highlighted in Figure 5, has a volume V given by:

$$V = \pi \left(\frac{D}{2} \sin \theta + r \right)^2 (D \cos \theta + 2r). \quad (31)$$

The figures of merit of this comparison are η_L , η_K and η_V , defined as:

$$\eta_L = \frac{J_{\text{equ,L}}}{J_{\text{std}}}, \quad \eta_K = \frac{J_{\text{equ,K}}}{J_{\text{std}}} \quad \text{and} \quad \eta_V = \frac{V}{V_{\text{std}}}. \quad (32)$$

These figures of merit describe the change in angular momentum, kinetic energy and volume between a standard flywheel and the flexure-based flywheel. These are given by:

$$\eta_L = \frac{4(1 - \cos \theta)}{(\xi^2 - 2\xi + 2)} \left[\frac{1}{5D^2} \left(\frac{6m}{\rho\pi} \right)^{\frac{2}{3}} + \frac{(\cos \theta + 1)}{2} \right], \quad (33)$$

$$\eta_K = \frac{8(1 - \cos \theta)}{(\xi^2 - 2\xi + 2)} \left[\frac{1}{5D^2} \left(\frac{6m}{\rho\pi} \right)^{\frac{2}{3}} + \frac{(\cos \theta + 1)}{4} \right] \quad (34)$$

and

$$\eta_V = \frac{\rho\pi\xi(2 - \xi)}{8m} \left(D \sin \theta + \left(\frac{6m}{\rho\pi} \right)^{\frac{1}{3}} \right)^2 \left(D \cos \theta + \left(\frac{6m}{\rho\pi} \right)^{\frac{1}{3}} \right). \quad (35)$$

The three figures of merit η_L , η_K and η_V are plotted in Figure 6-8, for masses $m = 0.1$ kg out of steel (density $\rho = 8000$ kg/m³). (Note: the range of D in these plots was selected to avoid interference of sphere shaped masses within dumbbell, as this would not be realistic.)

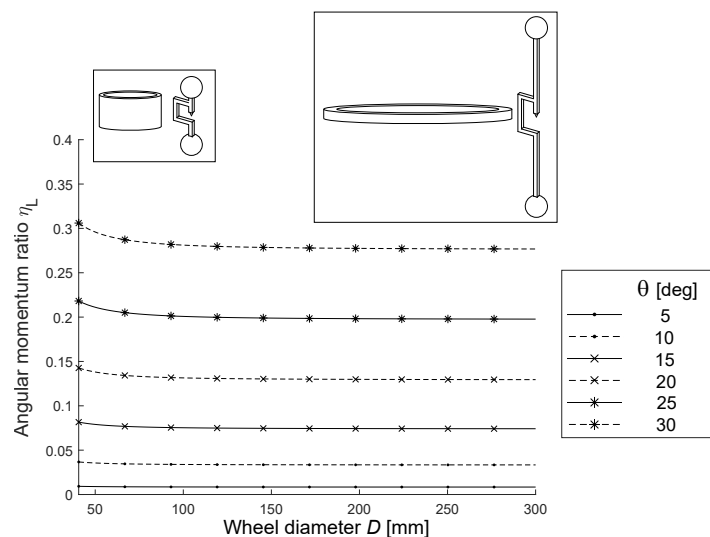


Figure 6. Angular momentum ratio η_L as a function of flywheel diameter D . The flywheel and dumbbell illustrations show the overall appearance for the different diameters D (not to scale).

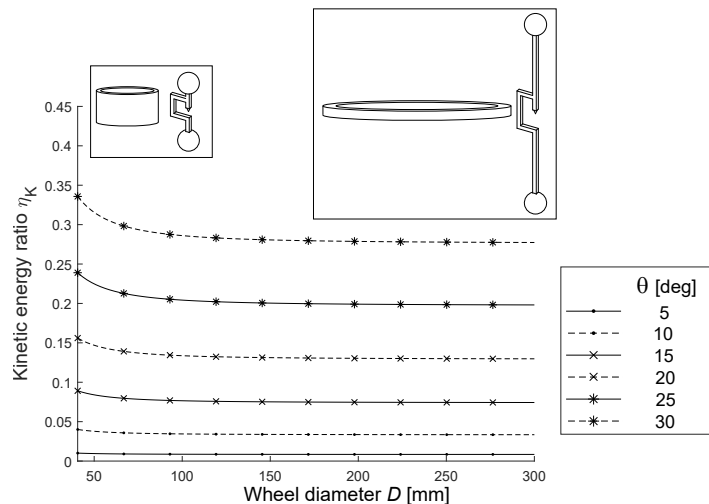


Figure 7. Kinetic energy ratio η_K as a function of flywheel diameter D . The flywheel and dumbbell illustrations show the overall appearance for the different diameters D (not to scale).

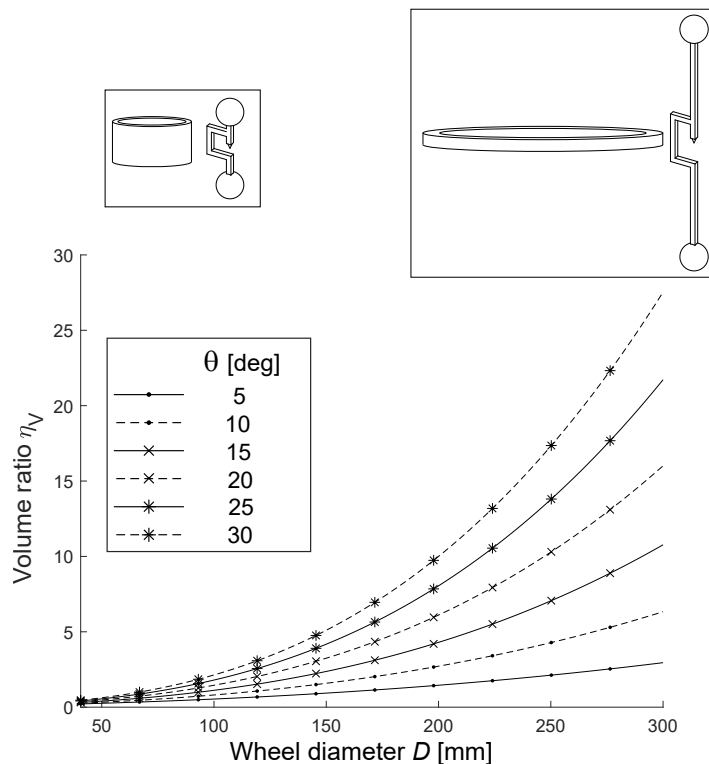


Figure 8. Volume ratio η_V as a function of flywheel diameter D . The flywheel and dumbbell illustrations show the overall appearance for the different diameters D (not to scale).

Eqs. (33) and (34) can be further simplified in the case of small masses m (or elongated dumbbells with large D). In this case, $\frac{m}{\rho} \simeq 0$, simplifying η_L and η_K to:

$$\eta_L \simeq \eta_K \simeq \frac{2 \sin^2 \theta}{\xi^2 - 2\xi + 2}. \quad (36)$$

It can indeed be seen in Figure 6 and 7 that, with the exception of the smaller diameters, the diameter D has little influence on η_L and η_K , as they depend mainly on θ . The conclusions to draw from the first two graphs are that even though increasing the size of the flexure-base design increases the kinetic

energy and angular momentum storage capacity, these keep the same proportion with respect to a standard flywheel. The only way to increase the storage capacity of this dumbbell design is to increase its tilt amplitude θ . All curves remain below one, meaning angular momentum and kinetic energy are always lower than for the equivalent flywheel. For the typical range of $\theta = 20^\circ$ for deflection of flexures (as this results in a deflection of 40° at the ball-joint), the kinetic energy and angular momentum lose almost an order of magnitude. As done for η_L and η_K , the same simplification can be applied to η_V :

$$\eta_V \simeq \frac{\pi D^3 \sin^2 \theta \cos \theta \rho \xi (2 - \xi)}{16m}, \quad (37)$$

and it can be seen that η_V increases with D^3 , also as seen in Figure 8. For the typical range of $\theta = 20^\circ$ of deflection on flexures and for a diameter D of 250 mm, it can be seen that the new design increases its volume by about an order of magnitude.

4. Influence of the Cylindrical Rigid Body Shape

Sect. 3 studied the influence of the flexure-based flywheel's size and tilt amplitude on its angular momentum and kinetic energy, allowing a comparison to be drawn with a standard flywheel. This section explores instead the effect of the shape of the cylindrical rigid bodies. The dumbbell design, though more realistic, will be left aside and pivoting cylinders (as shown in Figure 9) are considered instead (As before, these cylinders are linked to the ground by CV-joints located at their centres of mass.). These cylinders have a radius R , a thickness t and a fixed mass m (Even though m has already been used to denote the sphere-shaped masses in Sect. 3, it will again be used here to avoid complex nomenclature.). Their shape will be parameterised by their *shape ratio* λ :

$$\lambda = \frac{R}{t}. \quad (38)$$

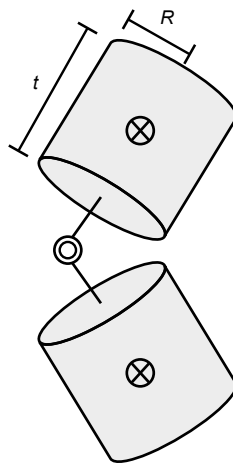


Figure 9. The studied pivoting cylindrical inertial bodies. As before, the cylindrical rigid bodies are fixed to the base via CV-joints and linked together via a ball joint.

The thickness t and radius R are given by:

$$t = \left(\frac{m}{\rho \pi \lambda^2} \right)^{\frac{1}{3}} \quad \text{and} \quad R = \left(\frac{\lambda m}{\rho \pi} \right)^{\frac{1}{3}}. \quad (39)$$

The resulting J_h and J_v are then (These are the well-known formulas for the moments of inertia of a cylinder around its principal axes.):

$$J_h = \frac{1}{12}m(3R^2 + t^2) = \frac{m}{12} \left[\left(\frac{m}{\rho\pi\lambda^2} \right)^{\frac{2}{3}} + 3 \left(\frac{\lambda m}{\rho\pi} \right)^{\frac{2}{3}} \right], \quad (40)$$

$$J_v = \frac{1}{2}mR^2 = \frac{m}{2} \left(\frac{\lambda m}{\rho\pi} \right)^{\frac{2}{3}} \quad (41)$$

The resulting $J_{\text{equ,L}}$ and $J_{\text{equ,K}}$ are given by:

$$J_{\text{equ,L}} = \frac{1}{6}(\cos\theta - 1)m \left(\frac{m}{\rho\pi\lambda^2} \right)^{\frac{2}{3}} (3\cos\theta\lambda^2 - 3\lambda^2 - \cos\theta - 1), \quad (42)$$

$$J_{\text{equ,K}} = \frac{1}{6}(\cos\theta - 1)m \left(\frac{m}{\rho\pi\lambda^2} \right)^{\frac{2}{3}} (3\cos\theta\lambda^2 - 9\lambda^2 - \cos\theta - 1). \quad (43)$$

The evolution of $J_{\text{equ,L}}$ and $J_{\text{equ,K}}$ with respect to λ is shown in Figs. 10 and 11 for a selection of elevation angles θ and with $m = 0.1$ kg out of steel ($\rho = 8000$ kg m⁻³):

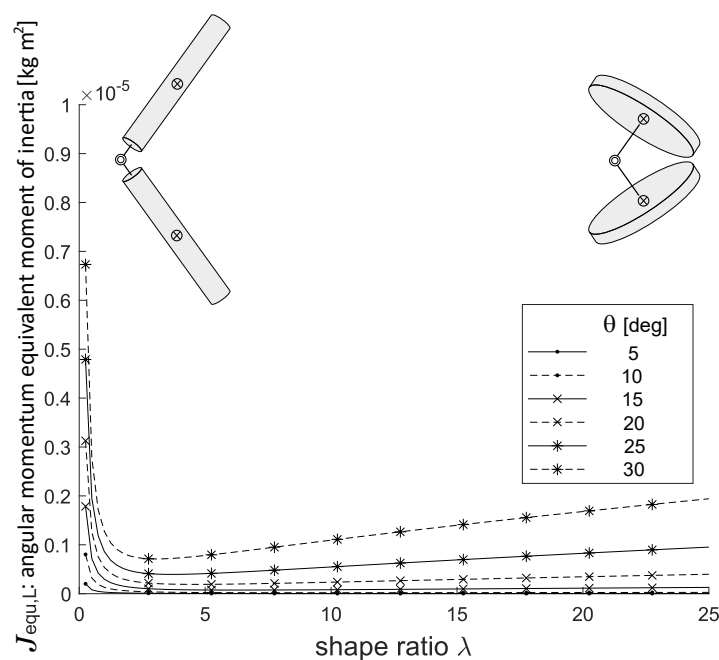


Figure 10. $J_{\text{equ,L}}$ as a function of shape factor λ . The two illustrations of the cylindrical inertial bodies show the overall appearance of the system for the different values of λ (not to scale).

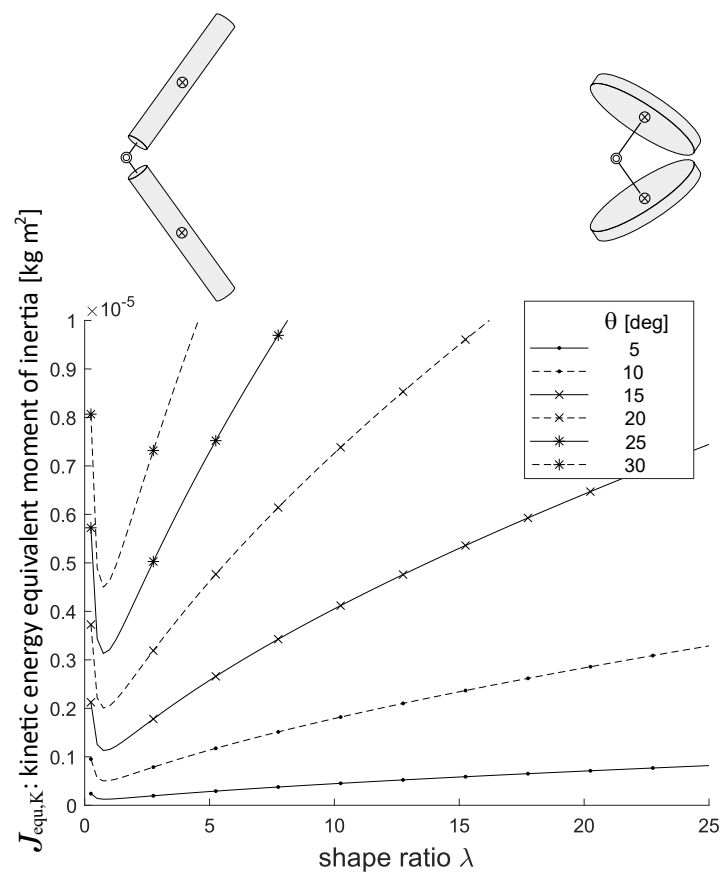


Figure 11. $J_{\text{equ,K}}$ as a function of shape factor λ . The two illustrations of the cylindrical rigid bodies show the overall appearance of the system for the different values of λ (not to scale).

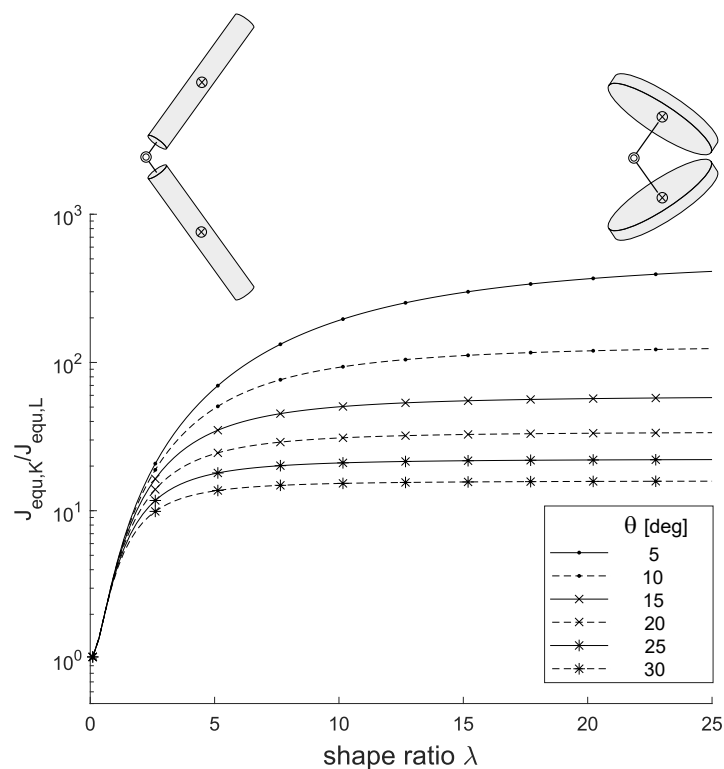


Figure 12. $J_{\text{equ,K}}/J_{\text{equ,L}}$ as a function of shape factor λ . The two illustrations of the cylindrical rigid bodies show the overall appearance of the system for the different values of λ (not to scale).

Figure 10 shows that the most angular momentum is generated with small values of λ , which corresponds to elongated slender cylinders. Large values of λ , which correspond to thin flat disks, result in little angular momentum, with a minimum for intermediate values. Intuitively explained, long slender cylinders and flat disks have the mass distributed from the centre of rotation, resulting in a larger angular momenta. For cylindrical inertial bodies that are neither slender nor flat, their mass is close to the centre, resulting in a smaller angular momenta. Last, it can be seen that increasing elevation angle θ increases the angular momentum.

Figure 11 shows that elongated slender cylinders store some amount of kinetic energy, but that flat disks store much more. There is also the same minimum for the same reason as for $J_{\text{equ,L}}$, in which cylindrical rigid bodies which are neither slender nor flat have their mass distribution closer to their centre of rotation. Similarly to $J_{\text{equ,L}}$, increasing θ also increases the stored kinetic energy.

The most striking result of Figure 12 is that the equivalent moments of inertia $J_{\text{equ,L}}$ and $J_{\text{equ,K}}$ are different. Indeed, for a standard flywheel, the same graph as Figure 12 would be a flat line $y = 1$. The fact that the ratio is not one means that the flexure-based flywheel can be seen as having two separate moments of inertia: one for storage of angular momentum and the other for storage of kinetic energy. Elongated cylinders have a ratio of approx. one, while thin flat disks have a ratio of approx. 100. This means that elongated cylinders have matching $J_{\text{equ,L}}$ and $J_{\text{equ,K}}$ and therefore behave identically to a standard flywheel. This joins the result of Eq. (36) because elongated dumbbells fall in the same category as elongated slender cylinders. Thin flat disks on the other hand, for the same amount of stored kinetic energy, generate approx. 100 times less angular momentum than a conventional flywheel would. This result leads to an interesting design consideration: if the goal of the flywheel is to generate angular momentum, then elongated cylinders are more better-suited, and if the goal is to store kinetic energy, then thin flat disks are optimal. This last property is interesting as it leads to reduced gyroscopic forces if the flywheel's axis is changed. Concerning the elevation angle θ , the ratio is larger for smaller elevation angles. This does not mean however that smaller elevation angles store more kinetic energy, but that they generate practically no angular momentum.

5. Analogy with a falling cat

It so happens that this flywheel design follows the mechanics of a falling cat which re-orient itself during its fall in order to land on its feet. Among the different models of a falling cat proposed by the literature [4–7], Rademaker [5] considers a falling cat as two rolling cylinders which keep a constant relative bending angle (Figure 13). Each cylinder has its own oblique and constant angular momentum (L'_1 and L'_2), resulting in a non-zero total angular momentum in the same manner as the proposed mechanism. Indeed, the two cylinders roll against each other without slipping, which implicitly assumes the presence of a CV-joint linking them.

A difference between Rademaker's model and the analysis presented in this work is the choice of the frame in which the angular momentum is evaluated. In Rademaker's case, this frame keeps the bend between the two cylinders in the same orientation. If the same falling cat is similarly described in a frame fixed with respect to the cat's waist, the two cylinders are no longer rolling around their respective axes, but perform the same pivoting motion of the proposed mechanism.

The falling cat phenomenon has already found several applications in robotics attitude control. However, examples of the literature [8–10] require motorised joints to provide the pivoting motion whereas this paper relies on passive mechanical means to guarantee the pivoting motion as well as the fixed elevation angle. Moreover, the presented mechanism follows truthfully the rolling cylinder model in contrast to other works in the literature [8,9], which use a Hooke joint instead of a CV-joint.

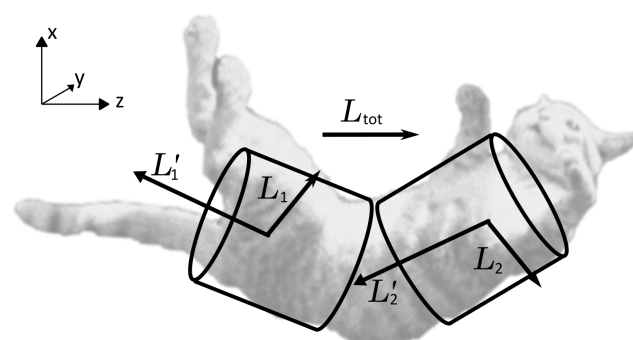


Figure 13. A falling cat seen as two rolling cylinders. In a frame where the cylinders rotate around their axes, they have angular momenta L'_1 and L'_2 . When in a frame fixed with respect to the cat's waist, the cylinders pivot and have angular momenta L_1 and L_2 which lead to an overall angular momentum L_{tot} . (Image adapted from [11])

6. Demonstrator prototype of the flywheel

6.1. Constructed demonstrator

A proof-of-concept demonstrator of the flywheel has been constructed with flexures and is shown in Figure 15. The CV-joints are constructed by means of a flexible rod parallel to the z -axis and a split flexible blade which lies in a plane parallel to the xy -planes (Figure 14a). The split blade, though technically overconstrained if considered as two independent blades, acts as a single blade and restricts translation in the x - and y -directions as well as rotation around the z -axis. The rod supports the mass in the z -direction and blocks its translation along that axis. It should be noted that the exactitude with which this flexure joint follows the kinematics of a CV-joint has not been investigated, as this joint is only used for a proof-of-concept demonstrator. The flexure ball joint consists in three askew flexible rods, as shown in Figure 14b. The first rod lies on the z -axis and restricts translation along this axis. The other two lie in two separate planes parallel to the xy -plane and restrict translation motion in the xy -plane (the separation between the planes by a distance d is to prevent collision between the two rods). The flywheel has a height of 400 mm, each rigid body has a weight of 1 kg and the CV-joints each have an amplitude of $\pm 12.5^\circ$ (the ball joint therefore has an amplitude of $\pm 25^\circ$).

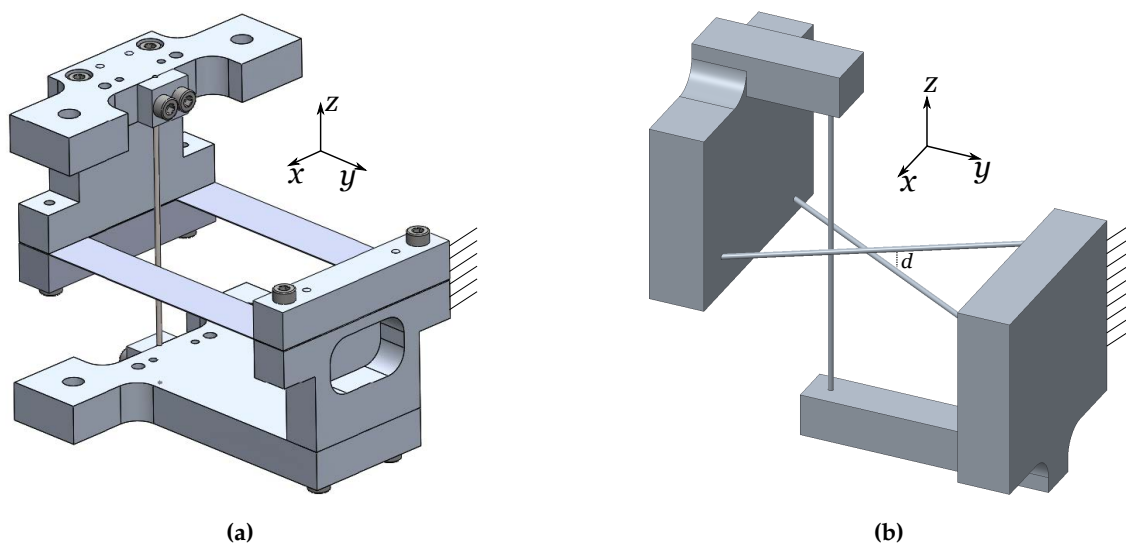


Figure 14. CAD views of the prototype's implemented flexure-based (a) CV-joint, which enables the upper part to pivot around the x - and y -axes, and (b) ball joint, which connects the two inertial pivoting bodies. Note: the two rods parallel to the xy -plane lie in two distinct planes separated by a distance d .

6.2. Experimental validation

To demonstrate that the physical demonstrator can generate angular momentum we propose to measure it while it is used as a reaction wheel (A reaction wheel is a device used in spacecrafts to control their orientation. It consists in a motorised flywheel which, when accelerated in one direction, accelerates the rest of the spacecraft in the other direction via a reaction torque.). The flywheel is used as reaction wheel in the sense that its base is free to rotate, resulting in conservation of angular momentum for the system consisting of the rotating base and flywheel. When an angular velocity variation $\Delta\dot{\varphi}$ is applied to the flywheel, this will result in a variation in the angular velocity of the base of opposite sign due to conservation of angular momentum.

6.2.1. Experimental setup

As the physical demonstrator only generates angular momentum along its z -axis, only the rotation of its base around this same axis is released. This was achieved with two ball bearings as illustrated in Figure 15. In order to actuate the flywheel, a stepper motor has been added to the demonstrator. Its stator along with its electronics are fixed to the flywheel's base while its rotor drives a pin attached to the lower part of Rigid body (2) by means of a slotted crank (Figure 16). One can observe that the angular velocity of the motor's rotor relative to its stator is equal to the parameter $\dot{\varphi}$ used in the calculation of the angular momentum of the flywheel, see Section 2.3. In order to measure the rotational speeds of both the rotor and the rotating frame, encoding wheels have been attached to them and are observed by a high-speed camera, fixed in the inertial frame, at a 500 Hz frequency. A video of this experiment can be found at <https://www.youtube.com/watch?v=tW9mJlxSyUs>. The motorized prototype as represented in Figure 15 has been set with the aforementioned elevation angle $\theta = 12.5^\circ$ and its principal moments of inertia are given in the following table:

Table 1. Principal moments of inertia of the demonstrator's moving parts.

Description	Name	Value [$\text{kg} \cdot \text{m}^2$]
Horizontal inertia of the pivoting body	J_h	$8.10 \cdot 10^{-3}$
Vertical inertia of the pivoting body	J_v	$8.54 \cdot 10^{-4}$
Vertical inertia of the frame	J_f	$3.03 \cdot 10^{-2}$
Vertical inertia of the rotor	J_m	$2.01 \cdot 10^{-5}$

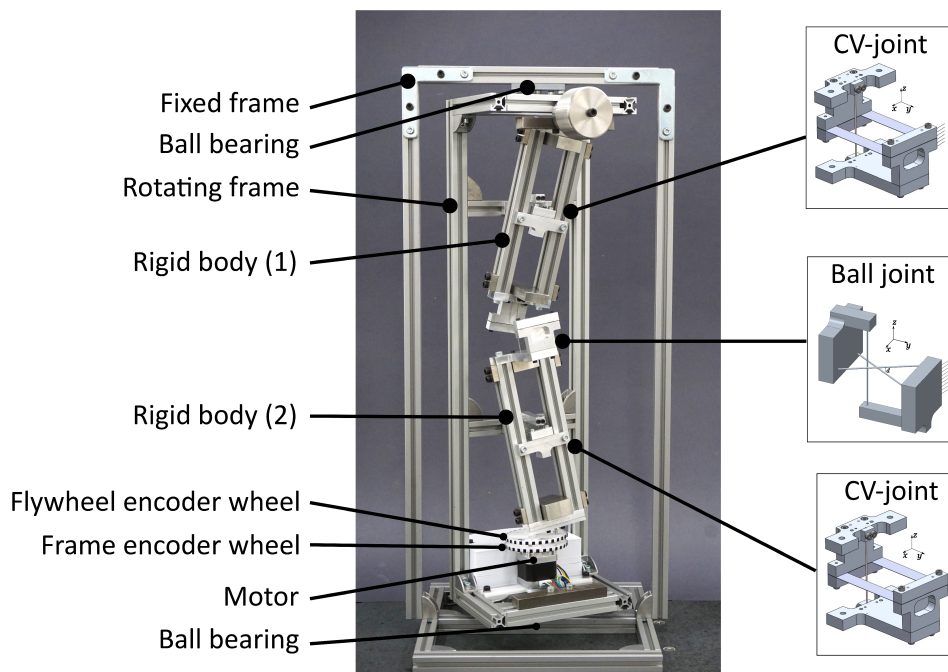


Figure 15. Constructed demonstrator with the different components and joints highlighted.

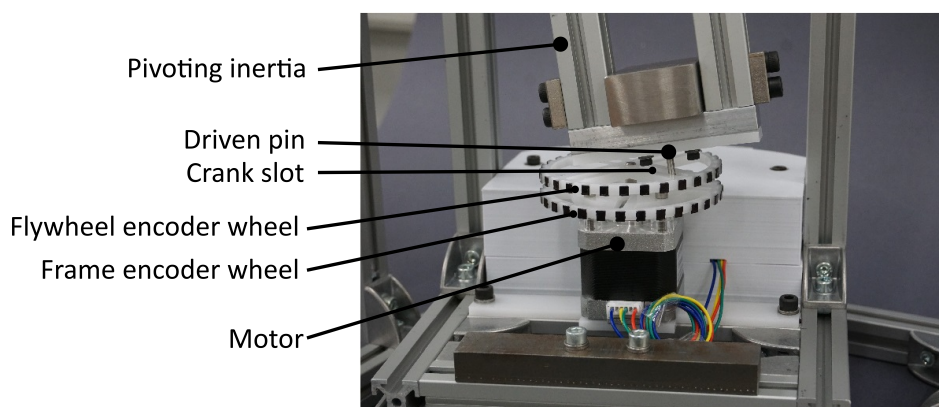


Figure 16. Measurement setup with the different components highlighted.

6.2.2. Experimental Results

The experimental measurements of the demonstrator are shown in Figure 17. The on-board rotor follows a repeating pattern: first, it accelerates to reach a positive speed of $3[RPS]$, then it maintains that speed, and finally, it brakes to return to zero speed. This sequence is then reversed, and the two phases are repeated in an alternating manner. For each acceleration and braking phase, we first compute the change of angular velocities of the rotor and the frame, noted $\Delta\dot{\phi}$ and $\Delta\dot{\alpha}$, respectively. Then, the corresponding speed ratios $\Delta\dot{\phi}/\Delta\dot{\alpha}$ are calculated in order to be compared with the expected speed ratio from Eq. (45). Note that we compute the speed ratios based on changes of speed rather than constant speed in order to be less dependent on friction, which tends to slow down the frame. The changes of angular velocities of the rotor and the frame and their corresponding speed ratio are gathered in Table 3.

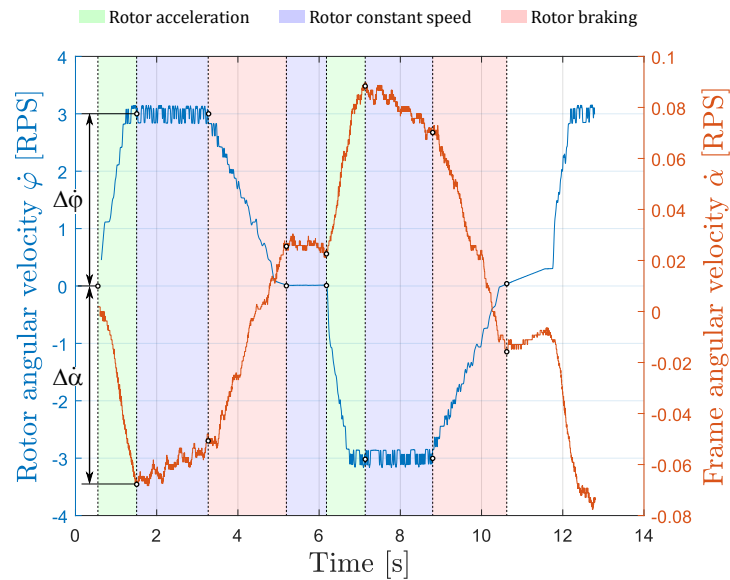


Figure 17. Angular velocities of the rotor ($\dot{\phi}$) and the frame ($\dot{\alpha}$) with respect to the time. The rotor acceleration, constant speed and braking phases are identified using green, blue and red colors respectively. The changes of angular velocity $\dot{\phi}$ and $\dot{\alpha}$ are highlighted for the first acceleration phase.

Table 2. Principal moments of inertia of the demonstrator's moving parts.

	Acceleration 1	Braking 1	Acceleration 2	Braking 2
$\Delta\dot{\phi}$ [RPS]	3.0	-3.0	-3.0	3.0
$\Delta\dot{\alpha}$ [RPS]	-0.0683	0.0776	0.0656	-0.0849
$\frac{\Delta\dot{\phi}}{\Delta\dot{\alpha}}$ [/]	-43.9	-38.7	-45.7	-35.3

Table 3. Changes of angular velocities of the rotor and the frame with their corresponding velocity ratios for the acceleration and braking phases of the rotor.

Considering the experimental set up presented in Figure 15, one can derive a formula that gives the speed ratio of the rotor's angular velocity over the rotating frame angular velocity under the assessment of angular momentum conservation. The full development is given in Appendix and the speed ratio that can be calculated is as follows:

$$\frac{\dot{\phi}}{\dot{\alpha}} = \frac{2(J_v - J_h) \cos^2 \theta + J_f + 2J_h + J_m}{2(J_h - J_v) \cos^2 \theta + 2J_v \cos \theta - 2J_h - J_m}. \quad (44)$$

By injecting into Eq. (44) the elevation angle and the moments of inertia given in Table 1 from the previous section, this leads to the expected speed ratio:

$$\frac{\dot{\phi}}{\dot{\alpha}} = -44.15. \quad (45)$$

The results from Table 3 shows a good agreement between the expected and measured speed ratios with a relative difference of 7.4%. One can observe that in average, the speed ratio's amplitude for the acceleration phases is 21% higher than the one from the braking phase. This difference can be explained by the presence of friction (bearings and air) which counteracts the frame's acceleration during the acceleration phases and helps to decelerate the frame during the braking phases.

7. Discussion and Conclusion

This article introduces a flexure-based mechanism that successfully meets the essential criteria for a flywheel. Indeed, it is able to store kinetic energy and a constant angular momentum at a constant

pivoting rate, it has a fixed centre of mass and has zero stiffness. A flexure-based implementation of the mechanism was shown, and the proof-of-concept prototype was successfully built and characterized in terms of reaction moment generation, which validates the analytical model.

In comparison to standard flywheels that use other types of bearings (such as ball bearings, magnetic bearings, and air bearings), the advantages of this flexure design are the absence of wear and lubrication, its low power consumption, its vacuum compatibility, and the possibility of miniaturisation. The price to pay for these advantages is a six-fold reduction in kinetic energy and angular momentum storage capacity for a given mass, as well as a ten-fold increase in volume.

A particularity of this flexure-based flywheel is that the shape of the pivoting rigid bodies influences the ratio of kinetic energy versus angular momentum stored in the mechanism. Rigid bodies with an elongated cylindrical shape have the same ratio as classical flywheels, whereas those that have the shape of a flat disk store up to 100 times more kinetic energy for the same angular momentum as classical flywheels. This could be advantageous for kinetic energy storage applications where angular momentum is undesired, for example, due to the induced gyroscopic forces.

Hence, although comparatively heavy and cumbersome, the novel flexure-based flywheel offers interesting design features that might be key to specific extreme-environment applications.

Acknowledgments: The authors would like to thank Ludovic Dauvin for his work in the construction of the prototype.

Appendix A

In this section, we develop the analytical model representing the experiment described in Section 6.2.

The approach is to study the system which contains all moving parts, which consist in the two pivoting rigid bodies, the rotating frame and the motor's rotor (which includes the driving crank). The system can be considered isolated as the external disturbances, such as friction in the rotating frame's bearings, are neglected. This assumption of an isolated system allows the conservation of angular momentum to be applied. As the system is at rest before switching the motor on, the angular momentum of the system must remain zero at all times.

The angular momentum is evaluated in \mathcal{R}_0 . As the frame's axis of rotation coincides with both the motor's axis and the pivoting centres of the rigid bodies, and as the rigid bodies pivot around their centres of mass, the centres of mass of each part remains fixed. This means that the angular momentum of each part can be evaluated in any inertial frame. For simplicity, the angular momenta of the pivoting inertias (1) and (2) are evaluated in frames \mathcal{R}_A and \mathcal{R}_B , respectively. The angular momenta of the rotating frame and motor rotor are evaluated anywhere on the z-axis.

The rotating frame's orientation (around the z-axis) is given by angle α and its angular velocity by $\dot{\alpha}$. The frame's centre of mass is centred on the z-axis and its moment of inertia, around the z-axis, is given by J_f (The other components of the rotating frame's inertia tensor need not be given, as they do not intervene in the calculation). The angular momentum \mathbf{L}_f of the rotating frame is then:

$$\mathbf{L}_f = J_f \dot{\alpha} \begin{bmatrix} 0 \\ 0 \\ 1 \end{bmatrix} \quad (\text{A1})$$

The motor's stator is fixed to the rotating frame and drives its rotor at a speed $\dot{\varphi}$ (which naturally imposes the same pivoting rate $\dot{\varphi}$ to the pivoting rigid bodies). The rotor and driving crank therefore have an angular velocity $\dot{\alpha} + \dot{\varphi}$ with respect to \mathcal{R}_0 . The motor's rotor has a moment of inertia J_m around the z-axis and its angular momentum \mathbf{L}_m is then:

$$\mathbf{L}_m = J_m (\dot{\alpha} + \dot{\varphi}) \begin{bmatrix} 0 \\ 0 \\ 1 \end{bmatrix} \quad (\text{A2})$$

Concerning the two pivoting rigid bodies, their rotation matrices need to be adjusted to include the rotating frame's motion. Rigid body (1)'s rotation matrix $\tilde{\mathbf{R}}_1$ is given by:

$$\tilde{\mathbf{R}}_1 = \mathbf{R}_z(\alpha)\mathbf{R}_{CV,1} = \mathbf{R}_z(\varphi + \alpha)\mathbf{R}_y(\theta)\mathbf{R}_z(-\varphi) \quad (\text{A3})$$

and rigid body (2)'s rotation matrix $\tilde{\mathbf{R}}_2$ is given by:

$$\tilde{\mathbf{R}}_2 = \mathbf{R}_z(\alpha)\mathbf{R}_{CV,2} = \mathbf{R}_z(\varphi + \pi + \alpha)\mathbf{R}_y(\theta)\mathbf{R}_z(-\varphi - \pi). \quad (\text{A4})$$

The rigid bodies' instantaneous angular velocities $\omega_{1,2}$ are then evaluated in \mathcal{R}_0 by using Eq. (7):

$$\omega_{1,2} = \dot{\varphi}(\mathbf{i} - \mathbf{v}) + \dot{\alpha}\mathbf{i} = \dot{\varphi} \left(\begin{bmatrix} 0 \\ 0 \\ 1 \end{bmatrix} - \tilde{\mathbf{R}}_{1,2} \begin{bmatrix} 0 \\ 0 \\ 1 \end{bmatrix} \right) + \dot{\alpha} \begin{bmatrix} 0 \\ 0 \\ 1 \end{bmatrix} \quad (\text{A5})$$

$$(\text{A6})$$

and their inertia tensors $\mathbf{J}_{1,2}$ are given by:

$$\mathbf{J}_{1,2} = \tilde{\mathbf{R}}_{1,2}\mathbf{J}_{\text{cyl}}\tilde{\mathbf{R}}_{1,2}^T. \quad (\text{A7})$$

Their angular momenta $\mathbf{L}_{1,2}$ are then:

$$\mathbf{L}_{1,2} = \mathbf{J}_{1,2}\omega_{1,2} \quad (\text{A8})$$

The angular momentum \mathbf{L}_{tot} of the complete system is given by:

$$\mathbf{L}_{\text{tot}} = \mathbf{L}_f + \mathbf{L}_m + \mathbf{L}_1 + \mathbf{L}_2 \quad (\text{A9})$$

$$= \begin{bmatrix} 0 \\ 0 \\ \dot{\alpha}((-2J_h + 2J_v)\cos^2\theta + J_f + 2J_h + J_m) - \dots \\ 2\dot{\varphi}((J_h - J_v)\cos^2\theta + J_v\cos\theta - J_h - \frac{J_m}{2}) \end{bmatrix} \quad (\text{A10})$$

As explained above, the system is isolated and $\mathbf{L}_{\text{tot}} = \mathbf{0}$. This means that the speed ratio $\dot{\varphi}/\dot{\alpha}$ is given by:

$$\frac{\dot{\varphi}}{\dot{\alpha}} = \frac{2(J_v - J_h)\cos^2\theta + J_f + 2J_h + J_m}{2(J_h - J_v)\cos^2\theta + 2J_v\cos\theta - 2J_h - J_m} \quad (\text{A11})$$

References

1. H. Schneegans and J. De Jong and F. Cosandier and S. Henein, Mechanism Balancing Taxonomy. *Mechanism and Machine Theory* **2023**, Elsevier
2. *Theory and design of spherical oscillator mechanisms*, I. Vardi, L. Rubbert, R. Bitterli, N. Ferrier, M. Kahrobaiyan, B. Nussbaumer, S. Henein, Precision Engineering 51 (2018), 499-513.
3. *Flexure wheels for spacecraft attitude control*, P. Flückiger, S. Henein, I. Vardi, H. Schneegans, L. Tissot-Daguette, EngrXiv pre-print (2021), DOI: <https://doi.org/10.31224/osf.io/trka6>
4. *Note relative à la communication de M. Marey*, M. Guyou, Comptes rendus de l'Académie des Sciences, vol.119, pp.717-718, 1894.
5. *Das Umdrehen der fallenden Katze in der Luft*, G. G. J. Rademaker, J. W. G. Ter Braak, Acta Oto-Laryngologica, vol.23, no.2, pp.313-343, 1936.
6. *A dynamical explanation of the falling cat phenomenon*, T. R. Kane, M. P. Scher, International Journal of Solids and Structures, vol.5, no.7, pp.663-670, July 1969.

7. *A Review of Research on Falling Cat Phenomenon and Development of Bio-Falling Cat Robot*, Cao & al., Proceedings of the 4th WRC Symposium on Advanced Robotics and Automation 2022, Beijing, China, September 20, 2022.
8. *Modular configuration design for a controlled fall*, T. W. Mather and M. Yim, 2009 IEEE/RSJ International Conference on Intelligent Robots and Systems, St. Louis, MO, 2009, pp.5905-5910.
9. *CatAstroΦ - Inertial reorientation of a freely falling cat using nonholonomic motion planning*, S. Crews & al., Biorobotics Laboratory, CMU, https://www.youtube.com/watch?v=_x5z8zz1uUE
10. *Design and Experimental Validation of Reorientation Manoeuvres for a Free Falling Robot Inspired from the Cat Righting Reflex*, Xavier Garant and Clément Gosselin, IEEE Transactions on Robotics, 2020, 10.1109/TRO.2020.3031241
11. A cat being dropped upside down, Ralph Crane, The LIFE Picture Collection, Shutterstock
12. *Large stroke high off-axis stiffness three degree of freedom spherical flexure joint*, M. Naves, R.G.K.M. Aarts, D.M. Brouwer, Precision Engineering, Volume 56, 2019, Pages 422-431, ISSN 0141-6359, <https://doi.org/10.1016/j.precisioneng.2019.01.011>.

Disclaimer/Publisher's Note: The statements, opinions and data contained in all publications are solely those of the individual author(s) and contributor(s) and not of MDPI and/or the editor(s). MDPI and/or the editor(s) disclaim responsibility for any injury to people or property resulting from any ideas, methods, instructions or products referred to in the content.